Melt Crystallization: Process Analysis and Optimization

Samuel W. Gilbert
Research Laboratories, Eastman Kodak Company, Rochester, NY 14650

Melt crystallization manufacturing systems are characterized mathematically and optimized. Directional solidification and sweating are modeled, and the results are correlated to plant data. A nonlinear programming algorithm is constructed to determine the optimal design and operation of a production plant. Process constraints include product purity, process yield, capital cost, phase equilibria, kinetic, and operational factors. An objective function is constructed from scaled yield and capital outlay formulae, and is optimized over a variably constrained feasible space. The dependence of the optima on the separation distribution coefficients and on the constraints is given for specific one-stage examples for three operational regimes. The one-stage analyses are applied for the solution of the n-stage problem.

Introduction

The chemical process industries are beginning to focus on manufacturing processes that address an enhanced environmental awareness on the part of the public and more stringent governmental regulations for chemical disposal and emissions. As a result, new separations technologies are being developed and implemented. Unit operations that minimize solvents and reduce operator exposure to chemicals are needed in today's chemical industries. An example of currently available technology is melt crystallization which offers unique separative potential for problematic and high-purity applications in addition to environmental and health benefits. As the industry concentrates its efforts more on the environmental and health aspects of chemical manufacturing, a better understanding of the processing aspects of melt crystallization is needed. This work addresses that need.

Melt crystallization is the separation process by which fractional separation is effected by directional solidification from the melt, usually without the use of solvents. The procedure can be utilized in a variety of ways: falling-film, shell-and-tube, cone, scraped surface, roll, screw and weir crystallizers, zone refiners, sweated pan apparatuses, and crystal washing devices.

In recent years, the chemical process industries have become more aware of the inherent advantages afforded by melt crystallization (Chowdhury, 1988; Genck, 1988; McCallion, 1989; Rittner and Steiner, 1985; Wynn, 1986). Although melt crystallization is not always the purification method of choice, it does have important processing, cost, and environmental advantages over the more conventional separations technologies.

This work describes models and a nonlinear programming algorithm for melt crystallization processes. Although the physics of melt purification are common to all processing techniques, the models of this work were developed to optimize two melt crystallization operations: static (Jancic, 1989; Nowicki et al., 1986) and dynamic (Sulzer Technical Publication, 1991; Mayer, 1974; Saxer, 1971; Ulrich, 1989). The goal is to develop the most cost-effective manner of preliminary plant design and operation, given the physical, thermophysical, and operational constraints inherent in each application.

The Process

Overview

An industrial static or dynamic melt crystallization system consists of a crystallizer, stage tanks, feed and product tanks, heat exchangers, pumps, and valves. Both processing modes are conducted in a semicontinuous, staged manner. Mass balance flowsheets of the process for one-stage and three-stage operations are shown in Figure 1. Although only one- and three-stage processes are shown, systems can be designed with any number of stages. For one-stage operation, production consists of the following steps:

Present address of S. W. Gilbert: Exxon Research and Engineering Company, P.O. Box 101, Florham Park, NJ 07932.

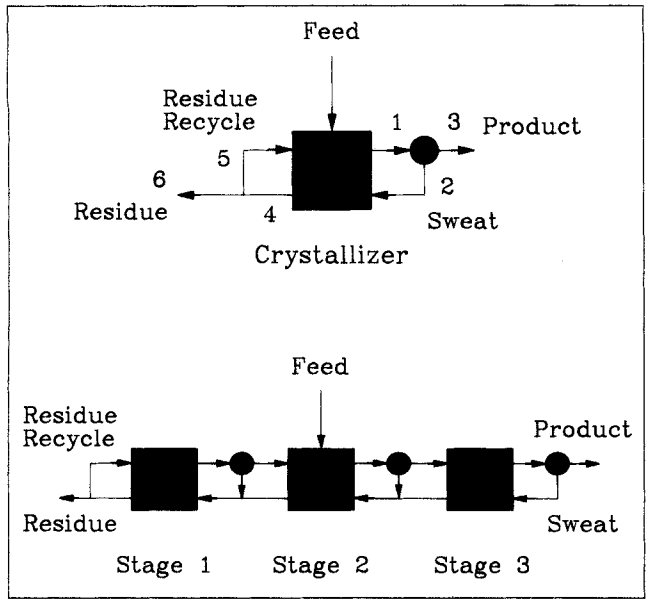

Figure 1. Mass balance diagrams for one- and three-stage processes.

Step 1. Molten feed is added to the crystallizer.

Step 2. The temperature of the crystallizer is lowered, inducing directional solidification.

Step 3. The residual mother liquor is drained.

Step 4. A portion of the residual mother liquor is removed from the process as residue.

Step 5. The crystals are sweated to induce fractional melting and further purification.

Step 6. The sweated crystals are melted and removed as purified product.

Step 7. The sweat fraction, the remaining portion of the residual mother liquors, and a fresh batch of feed are added to the crystallizer.

Step 8. Steps 1-7 are repeated (Sulzer Technical Publication, 1991; Saxer, 1971; Saxer and Papp, 1980; Ulrich, 1989; Wynn, 1986).

Industrial apparatus

An advantage of the static and dynamic modes is the fact that all mass and impurity flows are experimentally determined concurrently during operation. However, the two modes differ in many ways.

Dynamic melt crystallizers are operated such that the melt, from which product is crystallized, is continuously mixed (Sulzer Technical Publication, 1991; Jancic, 1986; Mayer, 1973, 1974; Saxer, 1971; Ulrich, 1989; Wynn, 1986). The separation achieved by a single static crystallization stage is approximately equivalent to two and one-half dynamic crystallization stages (Jancic, 1989). The advantage of the dynamic mode is the much lower capital and operating costs afforded by high inventory turnover (Wynn, 1986). For this reason, almost all production plants in current operation are dynamic. The falling-film dynamic process is staged such that crystals form against the crystallizer surface from a falling film of melt (Jancic, 1989; Mayer, 1973, 1974; Saxer, 1971, 1980; Saxer and Papp, 1980; Wynn, 1986).

Static melt crystallization can be performed with a single heat exchanger, tanks, pumps and valves. Although shell-and-tube exchangers are most common (Nowicki et al., 1986), scraped-wall, finned, and plate-and-frame exchangers have been used successfully (Shock, 1981). An example of such an arrangement is a tilted or vertical shell-and-tube exchanger fitted with pumps, valves, and a heat transfer circulating system on the shell side. Product is crystallized on the inside surface of the tubes, and mother liquor, sweat, and product are drained through a valve located beneath the apparatus. A shell-and-tube heat exchanger arrangement was used to purify naphthalene (Nowicki et al., 1986).

Suspension crystallization is another melt crystallization technology which is most applicable for high-duty separations with product melting points of less than 150°C (Nofsinger Technical Literature, 1991; Arkenbout, 1978; Genck, 1988; Matz, 1980a,b, 1981; McCallion, 1989; Shock, 1981). This work does not describe suspension crystallization.

Design and operation

Modeling and optimization provide insight as to the most cost-effective manner of plant design and operation. The following data are required for design and operation: desired product purity, duty, a range of feedstock compositions, impurity identities and phase diagrams, approximate ranges of product selling prices and feedstock costs, and minimum acceptable rates of return.

To determine the optimal design and operation of a melt crystallization facility, the designer must develop an understanding of the relationship between overall yield and total outlay. In this work, it is assumed that: (1) capital outlays greatly exceed several years' total operating expenses; (2) the capital cost of the facility scales proportionally with the size of the crystallizer; and (3) the size of the crystallizer scales proportionally with the mass crystallized. Although these assumptions are rudimentary, they provide an accurate basis for preliminary design. The accuracy results primarily because the capital required for the crystallizer constitutes the majority of the total outlay. The mass of product crystallized is directly proportional to the surface area available for crystallization, and the crystallizer size is proportional to the available surface area. Energy costs are low for melt crystallization, and the process runs with minimum supervision. Consequently, capital expenses dominate operating expenses.

Phase diagrams

The equilibrium solid-liquid thermodynamic behavior of organic mixtures is well documented (Sloan and McGhie, 1988). Binary organic mixtures usually exhibit eutectic, eutectic with limited solid solubility, or solid solution behavior.

Two types of limit, one thermodynamic and the other kinetic, can be imposed. A eutectic provides a thermodynamic constraint on the residue concentration. An even more stringent limit can be imposed by slow nucleation kinetics. At a relatively high concentration of impurity, melt may not crystallize within the time scale required.

Equilibrium-phase envelopes can be approximated linearly and with sophisticated empirical expressions. Linearization gives:

$$k \equiv \frac{C_s}{C_l} = \text{constant} \tag{1}$$

A set of linear approximations can be used to produce a more accurate representation of data over a large concentration range.

Since melt crystallization occurs far from equilibrium, the resultant solid phases contain significant amounts of impurity. Linearization of operating data gives:

$$k_{c,\text{eff}} \equiv \frac{C_s}{C_l} = \text{constant} \tag{2}$$

Melt crystallization and sweating distribution coefficients must be obtained experimentally using production equipment (Mayer, 1973, 1974; Saxer and Papp, 1980; Sloan and McGhie, 1988). Separation efficiencies depend strongly on the rate of interfacial advance and the processing mode. The static and dynamic modes of operation do not yield identical results; furthermore, variations in temperature gradients, flow rates, and apparatus geometry can produce large variations in results.

The Model

Melt crystallization

Although melt crystallization proceeds in a directional manner (from nuclei on a surface unidirectionally away from the surface), a nondirectional model can be used to describe many macroscopic aspects of the process. Fractional separation is initiated when, at an appropriate temperature, infinitesimally small crystals form on the crystallizer surface. At all times, the sum of the total liquid mass and the total crystal mass is constant and equal to the feed total liquid mass,

$$M_{l,0} = M_l + M_s \tag{3}$$

The notation used here is that of Saxer and Papp (1980). Differential total mass and impurity balances are:

$$dM_l + dM_s = 0 \tag{4}$$

$$d(C_l M_l) + d(C_s M_s) = 0 \tag{5}$$

Substitution and integration from the initial conditions to conditions obtained during the process give:

$$\frac{C_l}{C_{l,0}} = \frac{1}{k_c + (1 - k_c)\left(\dfrac{M_l}{M_{l,0}}\right)} \tag{6}$$

where k_c is the ratio of crystal and liquid impurity weight fractions present across the crystallization interface or the local melt crystallization distribution coefficient. This distribution coefficient is not the distribution coefficient indicated by the equilibrium-phase diagram. Industrial crystal growth rates greatly exceed the extremely slow rates required for near-equilibrium efficiency. Rearrangement of Eq. 6 gives:

$$\frac{M_l}{M_{l,0}} = \frac{\left(\dfrac{C_l}{C_{l,0}}\right) k_c - 1}{\left(\dfrac{C_l}{C_{l,0}}\right)(k_c - 1)} \tag{7}$$

and

$$k_c = \frac{\left(\dfrac{C_l}{C_{l,0}}\right)\left(\dfrac{M_l}{M_{l,0}}\right) - 1}{\left(\dfrac{C_l}{C_{l,0}}\right)\left(\dfrac{M_l}{M_{l,0}} - 1\right)} \tag{8}$$

An overall bulk impurity distribution coefficient k_c^* is defined as the ratio of the weight fraction of impurities in the bulk crystallized solid to the weight fraction of impurities in the bulk mother liquor:

$$k_c^* = \frac{C_{l,0} M_{l,0} - C_l M_l}{(M_{l,0} - M_l) C_l} = k_c \tag{9}$$

Sweating

Treatment of sweating is analogous to that of melt crystallization. Similarly,

$$M_{k,0} = M_k + M_l \tag{10}$$

Differential total mass and impurity balances are:

$$dM_k + dM_l = 0 \tag{11}$$

$$d(C_k M_k) + d(C_l M_l) = 0 \tag{12}$$

Substitution and integration from the initial conditions to conditions obtained during sweating give:

$$\frac{C_k}{C_{k,0}} = \frac{k_s}{1 - (1 - k_s)\left(\dfrac{M_k}{M_{k,0}}\right)} \tag{13}$$

where k_s is the ratio of crystal and liquid impurity weight fractions present across the sweating interfaces or the local sweating distribution coefficient. Similarly,

$$k_s^* = k_s \tag{14}$$

One-stage formulation

A flowsheet is shown in Figure 1. Let a_f be the total feed mass and w_f be the feed impurity weight fraction. The impurity can be envisioned as a single component or a mixture of several impurities—a pseudocomponent. Let a_i, $i = 1,6$ and w_j, $j = 1,6$ ($w_6 = w_5 = w_4$) be the stream total masses and stream impurity weight fractions, respectively. The crystallizer total mass balance is:

$$a_f + a_2 + a_5 - a_1 - a_4 = 0 \tag{15}$$

The sweating total mass balance is:

$$a_1 - a_2 - a_3 = 0 \tag{16}$$

and the residue recycle total mass balance is:

$$a_4 - a_5 - a_6 = 0 \tag{17}$$

Three independent variables are: the fraction of feed mass to the crystallizer that is crystallized prior to sweating q_c; the fraction of crystallized mass that is sweated q_s; and the fraction of residue that is recycled to the crystallizer q_r. If q_c, q_s, and q_r are specified, the steady-state mass and impurity balances are satisfied uniquely. The crystallizer total mass balance is:

$$a_1 - q_c(a_f + a_2 + a_5) = 0 \tag{18}$$

The sweating total mass balance is:

$$a_2 - q_s a_1 = 0 \tag{19}$$

and the residue recycle total mass balance is:

$$a_5 - q_r a_4 = 0 \tag{20}$$

The crystallizer and sweating impurity mass balances are:

$$a_f w_f + a_2 w_2 + a_5 w_4 - a_1 w_1 - a_4 w_4 = 0 \tag{21}$$

$$a_1 w_1 - a_2 w_2 - a_3 w_3 = 0 \tag{22}$$

Impurity distribution balances for crystallization and sweating are:

$$w_1 - k_c^* w_4 = 0 \tag{23}$$

$$w_3 - k_s^* w_2 = 0 \tag{24}$$

Substitution of the expressions obtained for a_i, $i = 1,6$ from the solution of Eqs. 15-20 into Eqs. 21-24 for w_j, $j = 1,4$ yields a system of four linear equations in four unknowns. The resultant set of solution formulae for a_i, $i = 1,6$ and w_j, $j = 1,4$ gives a complete characterization in terms of q_c, q_s, and q_r and parameters a_f, w_f, k_c, and k_s.

An outline of the formulation and solution for the n-stage system is included in the Appendix. Although not included in this work, analytical and numerical solutions have been obtained for multistage systems.

One-stage solution

The solution of the equations of the preceding section can be obtained by series techniques or elimination. The series solution is less tedious and reveals the structure of the solution. Details are given in the Supplementary Material. The solution to Eqs. 15-20 is:

$$a_1 = \frac{a_f q_c}{1 - \phi} \tag{25}$$

$$a_2 = q_s a_1 \tag{26}$$

$$a_3 = (1 - q_s) a_1 \tag{27}$$

$$a_4 = \left(\frac{1 - q_c}{q_c}\right) a_1 \tag{28}$$

$$a_5 = q_r a_4 \tag{29}$$

$$a_6 = (1 - q_r) a_4 \tag{30}$$

where

$$\phi = q_c q_s + (1 - q_c) q_r \tag{31}$$

The solution of Eqs. 21-24 is:

$$w_1 = \frac{w_f k_c^*}{[1 - q_c(1 - k_c^*)]} \cdot \frac{(1 - \phi)}{(1 - \gamma)} \tag{32}$$

$$w_2 = \frac{w_1}{k_s^* + q_s(1 - k_s^*)} \tag{33}$$

$$w_3 = k_s^* w_2 \tag{34}$$

$$w_4 = \frac{w_1}{k_c^*} \tag{35}$$

where

$$\gamma = \frac{\dfrac{q_s}{k_s^* + q_s(1 - k_s^*)} + \left(\dfrac{q_r}{k_c^*}\right)\left(\dfrac{1 - q_c}{q_c}\right)}{1 + \left(\dfrac{1}{k_c^*}\right)\left(\dfrac{1 - q_c}{q_c}\right)} \tag{36}$$

Identical formulae were obtained using MACSYMA version 412.61. Expressions for the partial derivatives of process yield, mass crystallized, stream total masses and impurity weight fractions were calculated with respect to variables q_c, q_s, and q_r.

Nonlinear programming

The general nonlinear, constrained optimization problem can be written as follows. Minimize $f(x)$ subject to

$$c_i(x) = 0, \quad i = 1, \ldots, k \tag{37}$$

$$c_i(x) \geq 0, \quad i = k+1, \ldots, m \tag{38}$$

where $f(x)$ is an objective function and constraints, and $c_i(x)$ are functions of n variables. FORTRAN-callable subroutine VMCOM, based on Powell's algorithm and earlier work by Han, allows solution of the problem (Crane et al., 1980).

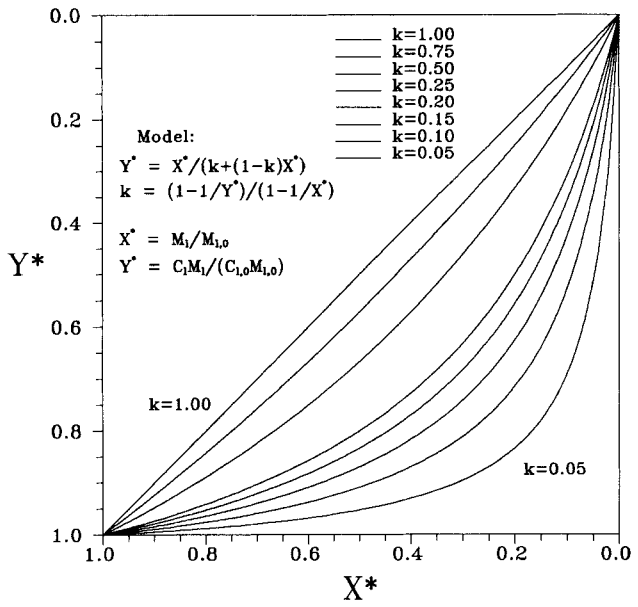

Figure 2. Melt crystallization model.

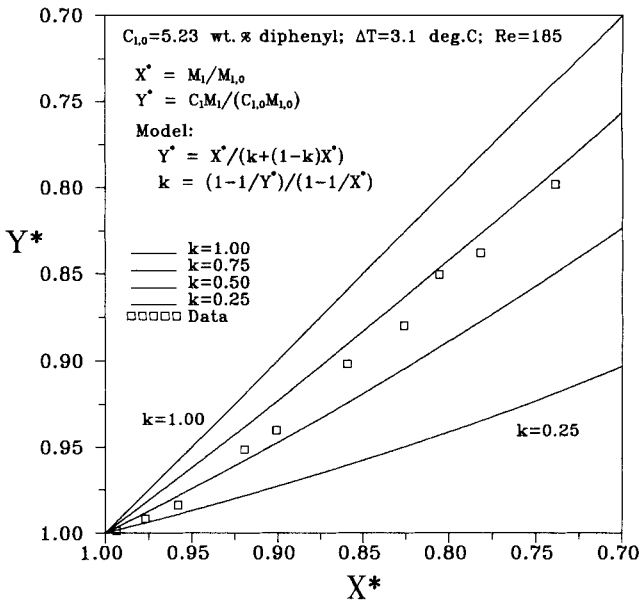

Figure 3. Fit of model to naphthalene melt crystallization data.

The objective function for the process is a linear combination of process yield and mass crystallized:

$$f(x) = -\alpha \cdot a_3(1 - w_3) + (1 - \alpha) \cdot a_1 \tag{39}$$

At a solution, the process yield proxy, $a_3(1 - w_3)$, is maximized, and the mass crystallized a_1 is simultaneously minimized. The solution where $\alpha = 1$ requires the yield to be maximized absolutely; the solution where $\alpha = 0$ requires the mass crystallized to be minimized absolutely.

The equality constraints are the total mass and impurity balances given by Eqs. 15-20, and crystallization and sweating distribution balances given by Eqs. 23 and 24. The inequality constraints are restrictions on the stream masses and weight fractions: stream masses are positive, $a_i > 0$; impurity weight fractions are positive and less than 1, $0 < w_i < 1$; the impurity weight fraction of stream 4 may not exceed the effective eutectic impurity weight fraction, $w_4 \leq w_{E,\text{eff}}$; the fraction of crystal sweated may not exceed a maximum; and the fraction crystallized may not exceed a maximum.

Feasible points are calculated using arbitrary, initial sets of process parameters q_c, q_s, and q_r, and the formulae given above. Subroutine VMCON is used to search the four-dimensional objective function surface for local and global minima. Calculations with random initial process parameter data sets and values of distribution coefficients are performed to answer the following questions:

- Are the optima unique?
- If not, are the optima unique in one or two of the operating parameters, q_c, q_s, and q_r? What are the contours of the optima in terms of the operating parameters?
- And most importantly, how should a process be designed and operated to produce quality product, maximize yield, minimize capital expense, and conform to all thermophysical, kinetic and operational constraints?

Results and Discussion

Melt crystallization

Phase concentrations, masses, and the distribution coefficient are related by Eqs. 3-9. The relationship between the relative purification and the fraction of initial charge remaining in the melt phase is shown in Figure 2 for various values of k_c. Coordinates X^* and Y^* are the ratio of melt-phase mass to the total mass and the ratio of melt-phase impurity mass to total impurity mass, respectively.

Figure 3 shows experimental data for falling-film melt crystallization of naphthalene (Mayer, 1973) and a fit of the model to the data. The data in Figure 3 were measured for an initial

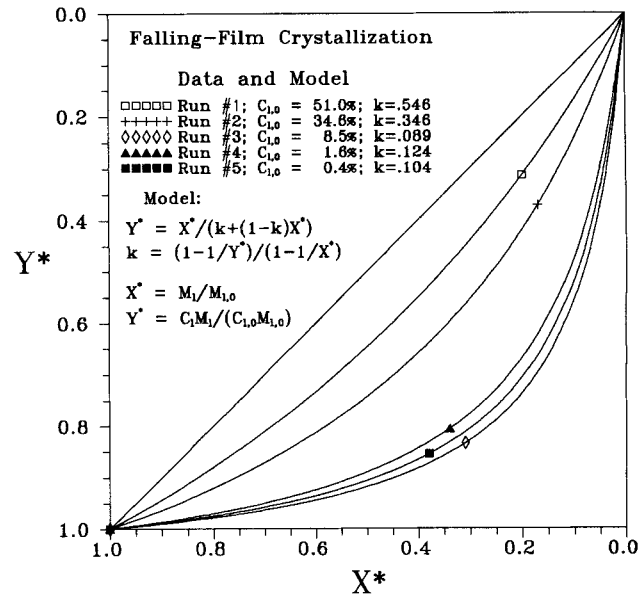

Figure 4. Fit of model to paraphenylenediamine melt crystallization data.

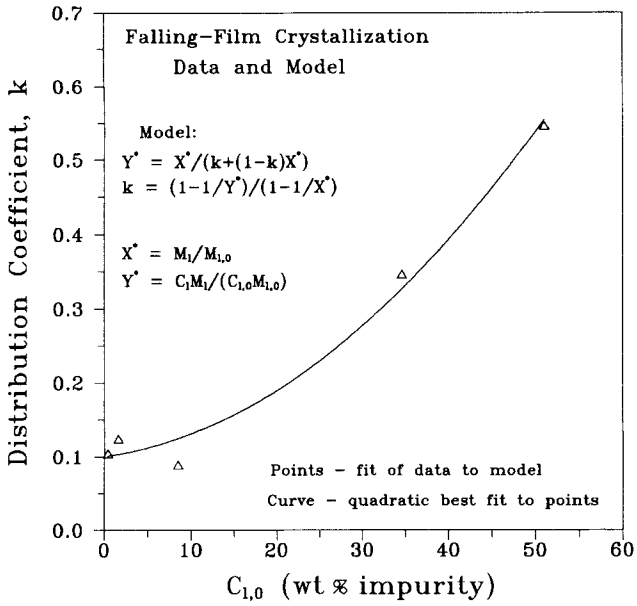

Figure 5. Fitted distribution coefficients for paraphenylenediamine melt crystallization data.

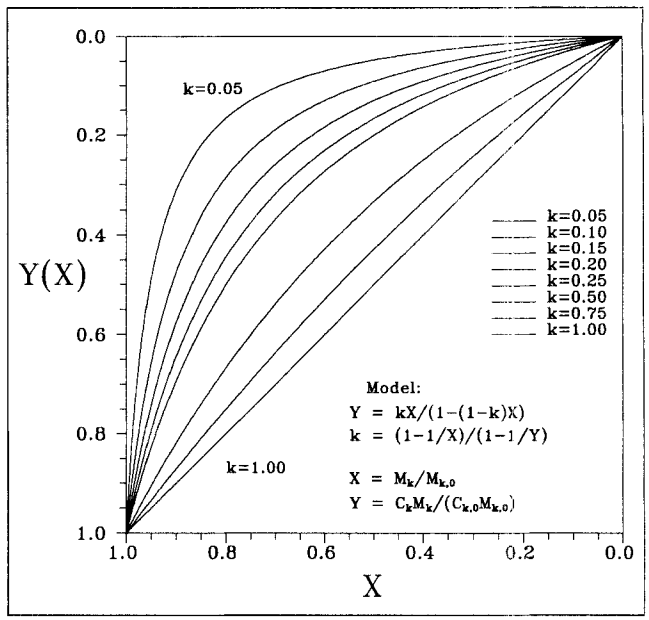

Figure 7. Sweating model.

melt containing 5.23 wt.% diphenyl at constant wall temperature gradient and film Reynold's number. The data are correlated accurately with k_c between 0.5 and 0.75. The fit of the model to melt crystallization data for naphthalene indicates that the model gives an accurate correlation up to a fraction crystallized q_c of approximately 0.25.

Data for falling-film melt crystallization of paraphenylenediamine are shown in Figure 4 (Saxer and Papp, 1980). Distribution coefficients were calculated using the data and Eq. 8. The fitted values of k_c shown for these data in Figure 5 indicate that purification is less efficient at higher concentrations of impurities.

Data for the falling-film melt crystallization of naphthalene are reproduced in Figure 6 (Mayer, 1973, 1974). Two trends are evident. As the initial melt impurity concentrations were increased at the constant crystal growth rate and wall temperature gradient, the distribution coefficients increased. Also, as the crystal growth rates were increased at constant initial melt impurity concentrations, the distribution coefficients increased.

The data and the fits to the data shown in Figures 4, 5 and 6 suggest that purification is most efficient when initial melts are relatively pure and when crystal growth rates are relatively low. These results are predicted by theories of crystal growth (Sloan and McGhie, 1988).

The data and their fits demonstrate that the purification efficiency of melt crystallization depends on initial melt con-

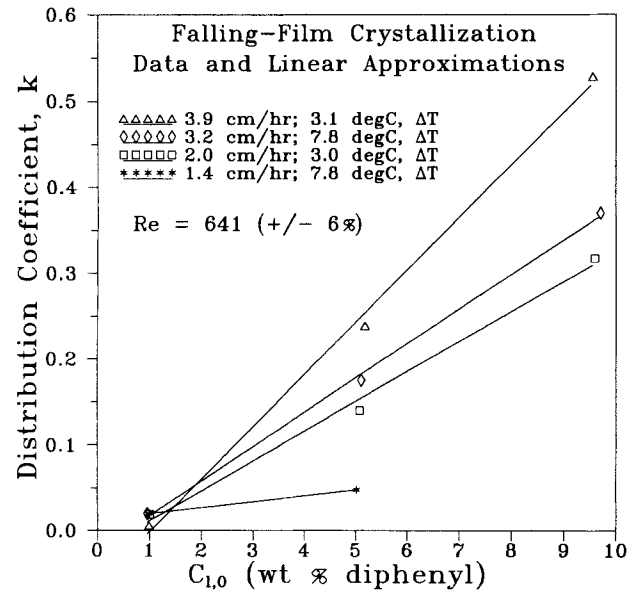

Figure 6. Experimental distribution coefficients for naphthalene melt crystallization.

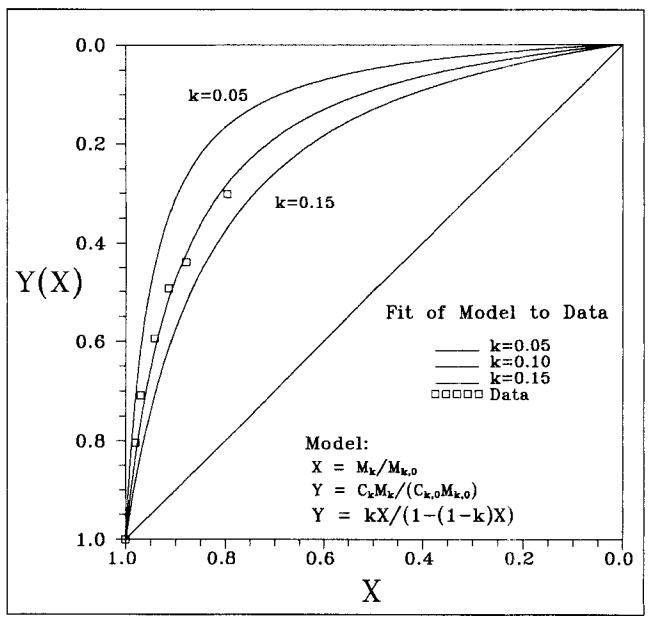

Figure 8. Fit of model to benzoic acid sweating data.

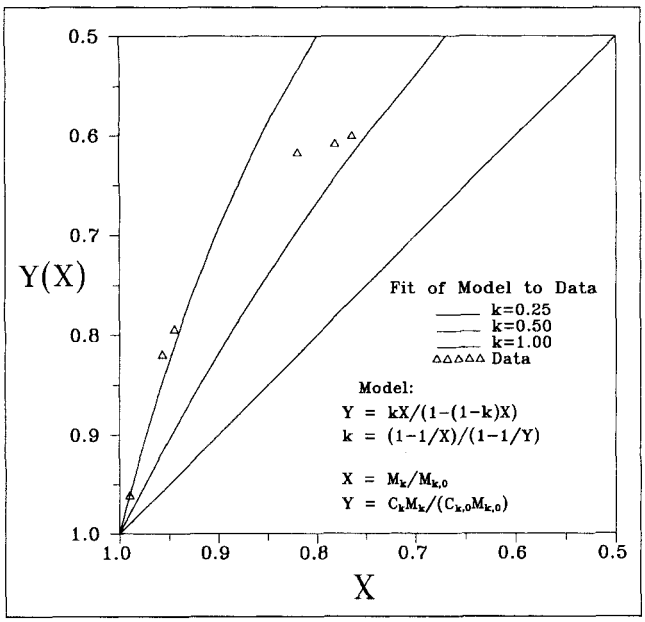

Figure 9. Fit of model to ϵ-caprolactam sweating data.

centration. For process optimization with variable feed concentrations, the model can be rationalized such that distribution coefficients are mapped directly into initial melt concentrations.

Sweating

The model of crystal sweating requires phase masses, concentrations, and the distribution coefficient to be related by Eqs. 10–14. The relationship between the relative purification and the fraction of initial charge remaining in the crystal phase is shown in Figure 7 for various values of k_s. Coordinates X and Y are the ratio of crystal-phase mass to the total mass and the ratio of crystal-phase impurity mass to total impurity mass, respectively.

Figure 8 shows experimental data and a fit of the model to the data for sweating of a benzoic acid mixture containing 20 impurities (Jancic, 1989). The unsweated crystal contained approximately 0.34 wt. % impurities and the final sweated crystal contained 0.13 wt. % impurities. The data are correlated accurately with a distribution coefficient equal to 0.10.

Data for sweating of ϵ-caprolactam (Ulrich, 1989) and a fit of the model to these data are shown in Figure 9. Although the data and the model correlation exhibit qualitative agreement, it is impossible to determine definitively the applicability of the model for quantitative correlation because of considerable scatter in the raw data.

Experimental data for sweating of paraphenylenediamine (Saxer and Papp, 1980) and fits of the model to the data are shown in Figure 10. Although the model is in qualitative agreement with the data, correlations for runs 3 and 5 are not quantitatively accurate. The correlated values of k_s demonstrate that, with the exception of run 5, paraphenylenediamine sweating efficiency increases as the initial crystal impurity concentration decreases.

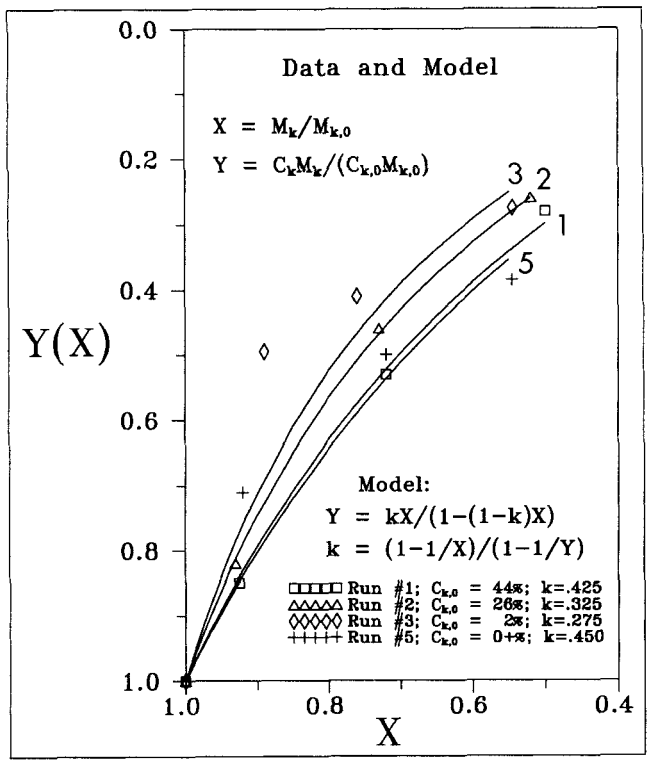

Figure 10. Fit of model to paraphenylenediamine sweating data.

One-stage system

Yield, product and residue masses and total mass crystallized per unit feed mass, and product and residue purities were calculated as functions of q_c and q_s using Eqs. 25–36 for $w_f = 0.10$, $k_c = k_s = 0.25$, and $q_r = 0.50$. Three-dimensional plots of these functions are given in the Supplementary Material.

Objective function and optima

For the analysis of the objective function and feasible space, it is convenient to reformulate the equations in terms of a different set of independent variables: w_3, w_4, and q_r. Mass and impurity balances for the system are:

$$a_f - a_3 - a_6 = 0 \tag{40}$$

$$a_1 - a_2 - a_3 = 0 \tag{41}$$

$$a_4 - a_5 - a_6 = 0 \tag{42}$$

$$a_1 - q_c(a_1 + a_4) = 0 \tag{43}$$

$$a_2 - q_s(a_2 + a_3) = 0 \tag{44}$$

$$a_5 - q_r(a_5 + a_6) = 0 \tag{45}$$

$$w_f a_f - w_3 a_3 - w_4 a_6 = 0 \tag{46}$$

$$w_1 a_1 - w_2 a_2 - w_3 a_3 = 0 \tag{47}$$

$$w_1 - k_c w_4 = 0 \tag{48}$$

$$w_3 - k_s w_2 = 0 \tag{49}$$

Equations 40 and 46 can be solved for a_3 and a_6 in terms of w_3 and w_4 such that:

$$a_3 = \frac{w_4 - w_f}{w_4 - w_3} a_f \tag{50}$$

$$a_6 = \frac{w_f - w_3}{w_4 - w_3} a_f \tag{51}$$

Equations 41 and 47 can be solved for a_1 and a_2 in terms of w_1, w_2, w_3, and a_3 giving:

$$a_1 = \frac{w_2 - w_3}{w_2 - w_1} a_3 \tag{52}$$

$$a_2 = \frac{w_1 - w_3}{w_2 - w_1} a_3 \tag{53}$$

The dependent variables are:

$$a_4 = \frac{a_6}{1 - q_r} \tag{54}$$

$$a_5 = q_r a_4 \tag{55}$$

$$q_c = \frac{a_1}{a_1 + a_4} \tag{56}$$

$$q_s = \frac{a_2}{a_2 + a_3} \tag{57}$$

Substitution of $k_c w_4$ for w_1 and w_3/k_s for w_2 into the expressions for a_1 and a_2 completes the reformulation. Variables a_1, a_2, a_3, a_6, and q_s are independent of q_r. Variables a_4, a_5, and q_c depend on w_3, w_4, and q_r.

The objective function, given by the righthand side of Eq. 39, depends only on a_1, a_3, and w_3, which are independent of q_r. Substitution of the reformulated expressions for a_1 and a_3 gives the objective function:

$$a_f \frac{(w_4 - w_f)}{(w_4 - w_3)} \left[-\alpha(1 - w_3) + (1 - \alpha) \frac{(w_3/k_s - w_3)}{(w_3/k_s - k_c w_4)} \right] \tag{58}$$

This expression is independent of q_r. Consequently, the solution to the optimization problem is a one-parameter family of solutions in q_r.

Feasible space

The bounded space available for minimization of the objective function can be represented two-dimensionally in w_3 and w_4. Figure 11 shows the feasible space. If the crystallization and sweating distribution coefficients are less than unity, as is the case for most organic systems, w_4 is constrained to be greater than w_f. Although the separations considered here do not include systems with distribution coefficients greater than unity, the model could be adapted for this type of application. Another limitation on w_4 is the thermophysical constraint imposed by a true eutectic or by poor crystallization kinetics. A eutectic bounds w_4 from above. If the system has no effective upper bound, the feasible range for the residue impurity weight fraction is $w_f < w_4 < 1$. If the system has an effective upper bound, then $w_f < w_4 \leq w_E$. Since salable products must meet a minimum level of purity, the constrained range imposed on w_3 is $0 < w_3 \leq w_p$.

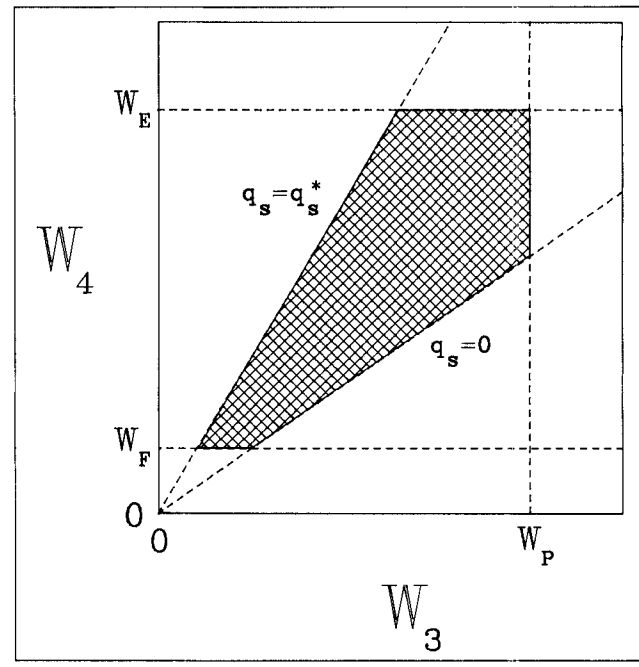

Figure 11. Feasible space.

Sweating imposes another constraint. Since crystals can be sweated only a certain amount before the crystal structure disintegrates, a bound is placed on the feasible space,

$$w_4 \leq \left[\frac{1}{k_c} + q_s^* \left(\frac{1 - k_s}{k_c k_s} \right) \right] w_3 \tag{59}$$

where q_s^* is the maximum sweating fraction. This inequality is derived by substitution of the expressions for a_3 and a_2 from Eqs. 50 and 53 into Eq. 57 relating q_s to a_3 and a_2. The natural bound on q_s such that $q_s \geq 0$ is represented as:

$$w_4 \geq \frac{w_3}{k_c} \tag{60}$$

The feasible space is bounded by $w_4 > w_f$, $w_4 \leq w_E$, $w_3 \leq w_p$, $q_s \geq 0$, and $q \leq q_s^*$. The line segment $\{(w_p, w_p/k_c^*), (w_p, w_E)\}$ represents feasible space that would allow the manufacture of product that just meets the minimum purity requirement. The line segment $\{(w_f k_c^*, w_f), (w_p, w_p/k_c^*)\}$ represents the space that would allow manufacture of product exceeding the minimum purity without sweating. There exists the special situation in which $w_E = w_p/k_c^*$. Although not likely to occur in practice, this case is the transition point between a locus of space satisfying the minimum product purity requirement and a locus that allows the manufacture of higher purity product. There also exists the case where $w_E < w_p/k_c^*$. This represents the highly constrained operation mandated by a low-impurity weight fraction eutectic.

Constant distribution coefficients

Unconstrained Operation. An example is useful for illustration of the method. A typical application might be separation of 90% feed into product of purity not less than 94%

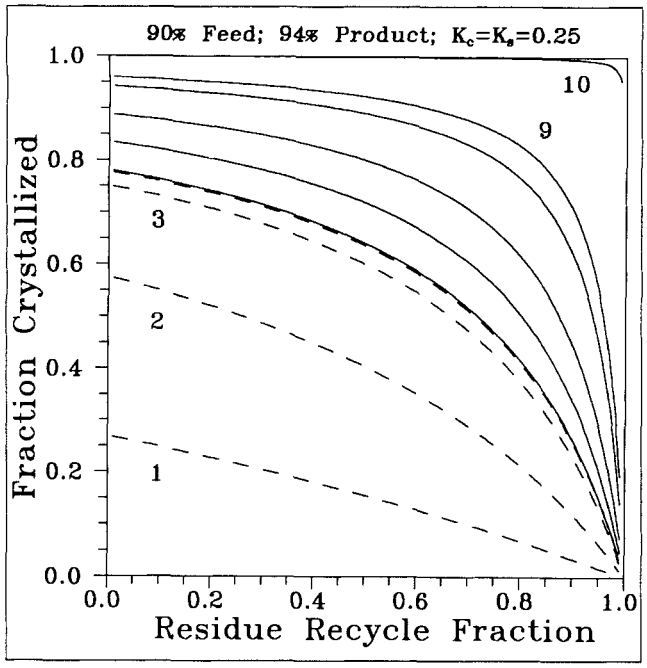

Figure 12. One-parameter family optima.

and residue. Crystallization and sweating impurity distribution coefficients are constant and equal to 0.25. The separation is not constrained by an effective eutectic, a maximum fraction sweated, or a fraction crystallized maximum.

The solution family is plotted with respect to q_r for various values of α in Figure 12. Figure 13 shows the optimized process yield, mass crystallized, residue purity, and the unique, optimal fraction sweated for the full range of α. Solutions of $\alpha < 0.510$ are not physically meaningful.

The solution consists of three operating regimes. The first regime, $0.510 \leq \alpha \leq 0.540$, corresponds to process designs favoring low capital costs and low overall yields ($\alpha = 0.510$ corresponds to the lowest capital cost and yield). For this range of α, the required yields are low, and the system can meet

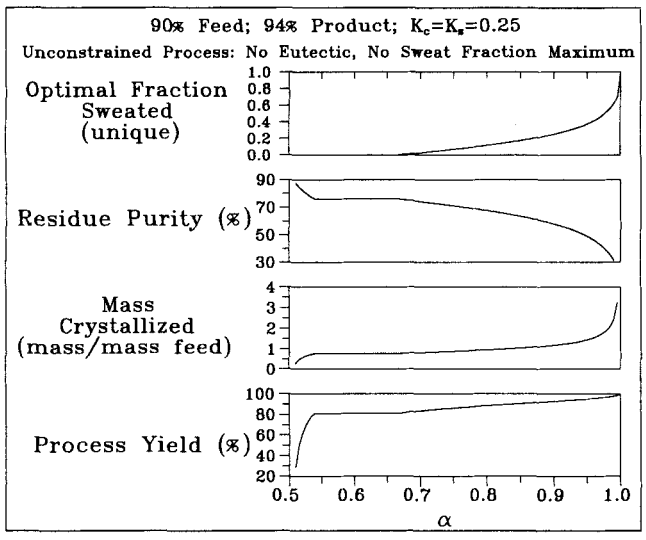

Figure 13. Process variable trends: no constraints.

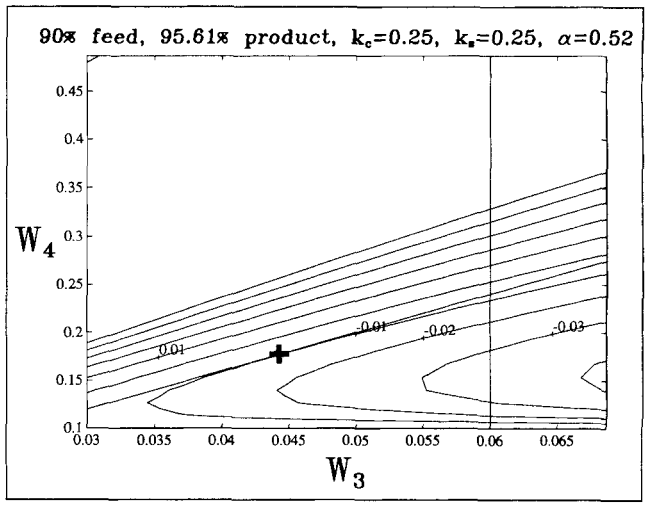

Figure 14. Objective function contour plot: $\alpha = 0.52$.

product purity without sweating. In fact, the yield requirements imposed in the first regime are so low that the product purity is greater than 94% for all α. Figure 13 shows that in this regime the yield and mass crystallized increase rapidly with α. Curves 1-3 shown in Figure 12 are the solutions corresponding to $\alpha = 0.510$, $\alpha = 0.520$, and $\alpha = 0.535$. These curves identify combinations of q_r and q_c that result equivalently in the optimized yield and capital outlay.

The second regime, $0.540 < \alpha < 0.665$, also indicates a design in which sweating is not required to reach 94% product. However, product purity in the second regime is exactly 94%. Curve 4 in Figure 12 corresponds to the second regime.

The third regime, $0.665 \leq \alpha \leq 1.000$, corresponds to higher yields where sweating is required. The mass crystallized per unit feed mass increases from 0.78 at $\alpha = 0.665$ to more than 3 above $\alpha = 0.980$. Product purity is exactly 94% for all values of α. Curves 5-10 in Figure 12 are the solutions for $\alpha = \{0.670, 0.750, 0.850, 0.950, 0.975, 1.000\}$. This regime is typical in manufacturing since required yields are usually in excess of those achieved by crystallization with no sweating.

Figures 14-17 show the objective function in contour as a

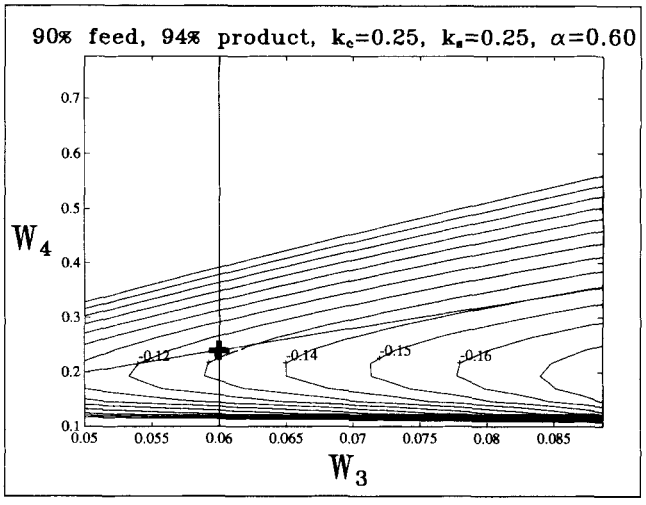

Figure 15. Objective function contour plot: $\alpha = 0.60$.

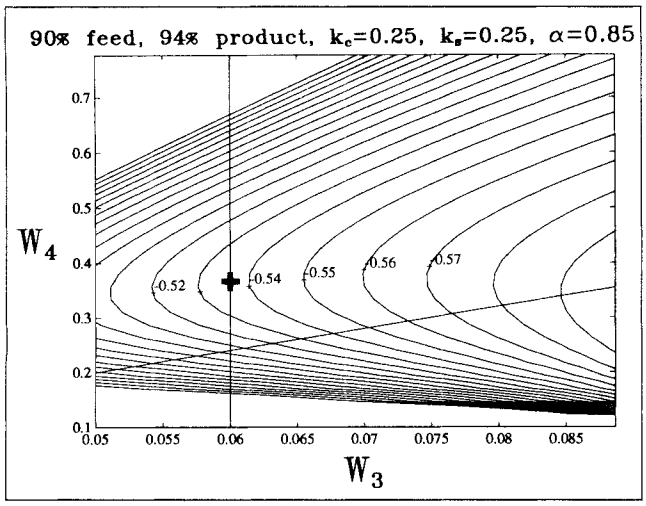

Figure 16. Objective function contour plot: $\alpha = 0.85$.

function of w_3 and w_4. Singularities are not shown on the plots. Two constraints are shown: $w_3 = 0.06$ and $q_s = 0$ (the line through the point $w_3 = w_4 = 0$ with slope $1/k_c$). A third constraint, the sweating fraction corresponding to $q_s = 1$ (the line through the point $w_3 = w_4 = 0$ with slope $1/[k_c k_s]$), ($q_s^* = 1$, Eq. 59) is shown in Figure 17. The feasible space is defined by:

$$\left\{(w_3, w_4): \quad w_3 \le 0.06, \quad w_4 \ge \frac{w_3}{k_c}, \quad w_4 < \frac{w_3}{k_c k_s}\right\} \tag{61}$$

As α is increased, the troughs of objective function contour minima shift toward higher values of w_4. Also, as α is increased, the troughs of minima become more negative with respect to fixed w_3 since the first term of expression 58 is negative and is proportional to α.

Figure 14 shows operation in the first regime. The minimum occurs on the boundary $q_s = 0$. Sweating is not necessary since the required yield is low, 61.16%. The product purity, 95.61%, is in excess of that required, 94%. As α is increased, the solutions move along the line $w_4 = w_3/k_c$. At $\alpha = 0.540$, the solution is the corner of the feasible space defined by the

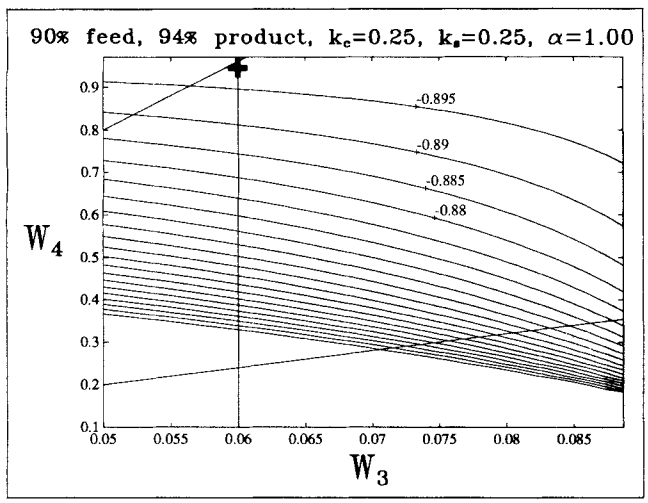

Figure 17. Objective function contour plot: $\alpha = 1.00$.

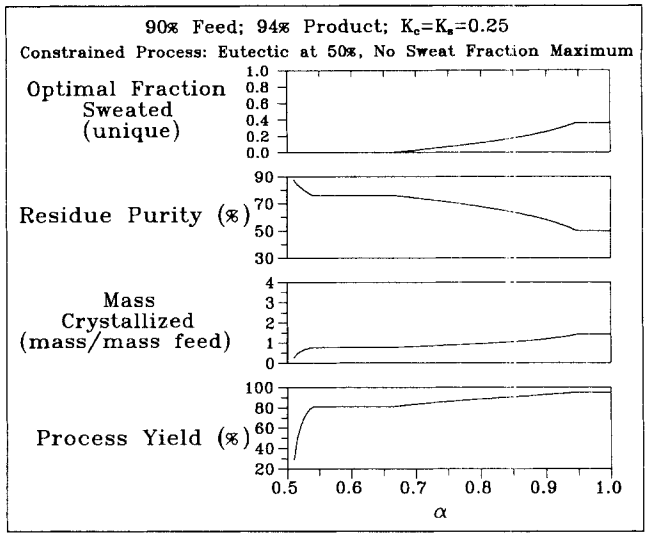

Figure 18. Process variable trends: eutectic constraint.

intersection of $w_3 = 0.06$ and $q_s = 0$. This marks the end of the first regime.

Figure 15 shows operation in the second regime. As α is increased, the troughs of objective function contour minima sweep in the direction of higher w_4 across the corner of the feasible space. When the centerline of the troughs passes the corner, the second regime ends.

Figures 16 and 17 show the objective function in the third regime. As α is increased, the troughs of contour minima shift toward higher w_4. The solutions for all α in the third regime are defined by the intersection of the boundary $w_3 = 0.06$ and the contour trough minima. Figure 17 shows the special case when $\alpha = 1.000$. Although not of practical value, this case is of theoretical interest. At $\alpha = 1.000$, no trough contours exist and the solution approaches the intersection of $w_3 = 0.06$ and $q_s = 1$. The fraction crystallized at the solution is 0.9900, the fraction sweated is 0.9899, and the fraction recycled is 0.9532. The mass crystallized approaches infinity (the crystallizer size and cost also approach infinity), and the residue purity approaches 0% (no eutectic).

Examples showing the effects of higher crystallization and sweating efficiencies on the optima are given in the Supplementary Material. Also given is an example where the product purity is required to be no less than 97 wt. %. It is shown that as the product purity is increased at constant separation efficiencies, the first and second regimes are diminished. At higher product purities, only the third regime is available for operation.

Constrained Operation. The process can be constrained by a eutectic, a sweating fraction maximum, or a crystallization fraction maximum. Figure 18 shows the process variables for the above example with a eutectic at 50 wt.% purity. At $\alpha = 0.945$, the process is constrained by the eutectic, and no higher yields are possible. Figure 19 shows the process variables for the original example with a sweat fraction maximum at 40%. At $\alpha = 0.960$, the yield is similarly constrained.

An example with a fraction crystallized maximum and examples with combinations of eutectic and fractions sweated and crystallized maxima are given in the Supplementary Material. Also given are examples identical to the above original

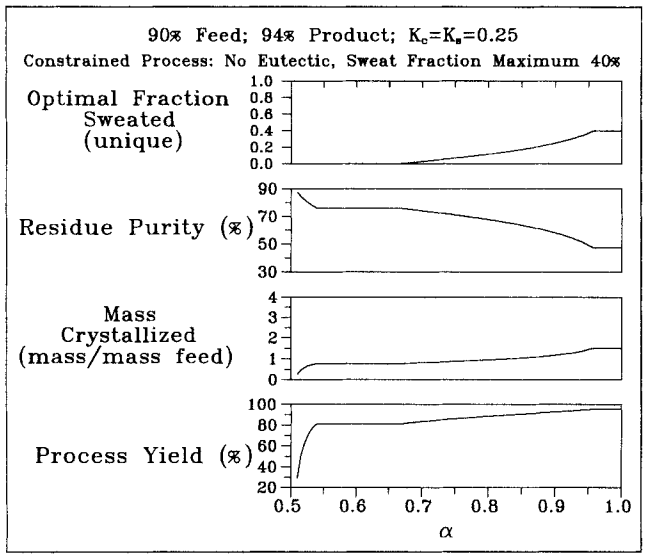

Figure 19. Process variable trends: sweating fraction constraint.

except that the product purity is required to be not less than 97 wt.%.

Variable distribution coefficients

The models and algorithm are valid without modification for separations with variable distribution coefficients. Falling-film melt crystallization and sweating experimental data for purification of paraphenylenediamine (Saxer and Papp, 1980) were correlated using the crystallization and sweating models (Figures 4, 5 and 10). The model was used to predict optimal design and operation for the full range of combined yield and capital outlay for the following separation: 90% feed, ≥97% product, and no eutectic or sweating constraints. Results are given in the Supplementary Material.

Outline of plant design

For the preliminary design, an understanding of the relationships between process yield and capital cost must be developed. An optimal design involves a balance of duty, capital outlay, and expenses associated with disposal, recovery, sale, or reuse of residue, subject to feedstock and required product purities, and thermodynamic, kinetic and operational constraints. Data needed are duty, minimum salable product purity or a range of purities, product sales price or a range of prices, feedstock cost or a range of costs, value of process residue, and costs of crystallizer and auxiliary tanks, pumps, valves and control equipment.

The crystallization and sweating impurity distribution coefficients, the system eutectic, if any, and maximum sweating fraction must be determined experimentally with plant equipment. It may be necessary for these data to be correlated and mapped to feed melt and crystal impurity concentrations.

The algorithm described in this article is used to determine qualitatively the optimal manner of operation. Understanding of the relationship between yield and capital outlay allows values of α to be correlated with combinations of yield and capital. A yield can be attained, given that the product satisfies the purity requirement, that the available supply of capital is not exceeded, and that the process satisfies the thermodynamic, kinetic and operational limitations.

The typical separation is constrained by eutectic or sweating fraction maximum. Yield can be increased at increased capital outlay, until one of the constraints is reached. When a particular combination of yield and capital outlay is identified as ideal, the residue recycle fraction and the fraction crystallized can be adjusted appropriately with no net effect on yield and outlay. The best design will utilize the appropriate combination of residue recycle and fraction crystallized.

Conclusions

The models of melt crystallization and sweating are self-consistent and correlate well with plant data. The programming algorithm incorporates the important considerations for process design and operation including yield, capital and residue costs, as well as eutectic, sweating and operational constraints.

The melt crystallization unit operations of fractional solidification and melting can be modeled mathematically, and the melt crystallization manufacturing process can be optimized for preliminary design and operation. The crystallization and sweating processes are described by simple differential equation models, and the resulting expressions relating melt- and solid-phase concentrations to fractions solidified and melted have single adjustable parameters, the distribution coefficients. The melt crystallization and sweating separations are correlated well by the models and the parameters correlate with the feed impurity concentrations. However, since the fits to the data are only qualitatively accurate, optimization using the models cannot be viewed as a quantitative guide for design.

Formulae relating melt- and solid-phase concentrations, the crystallized and sweated mass fractions, and the distribution coefficients were incorporated into a model of the manufacturing process. A nonlinear programming algorithm was used to optimize the operation of the crystallization system. The objective function is a nonlinear function of two independent variables and is minimized over a variably constrained feasible space. Equality constraints are the process mass balances. Inequality constraints include the minimum product purity, maximum sweating fraction, and the effective eutectic composition for the system. The solution is shown to be a one-parameter family of solutions. The most natural parameter for the solution families was demonstrated to be the residue recycle fraction, and the complete solution is a continuous family of loci, unique in optimal sweated fraction, but nonunique in the residue recycle fraction. It was shown that the solution of the n-stage system is an analogous one-parameter family in the residue recycle fraction. Consequently, the analyses for the one-stage system can be applied for the n-stage system.

The process can be operated optimally in three distinct regimes. The first regime is indicated when sweating is not necessary to meet the yield and product purity requirements. In these cases, capital outlay is low and the product purity is greater than that required. In the second regime, sweating is not required and product purity does not exceed the minimum. It is the transition between the first and third regimes. In the third regime, sweating is required to achieve the minimum product purity.

Acknowledgment

Collaboration with Dr. Kam-Chuen Ng of the Eastman Kodak Research Laboratories is greatly appreciated.

Notation

a = vector of process flowsheet stream masses
a^m = stage m vector of flowsheet stream masses, $m=0, n$
a_f = process feed total mass
a_f^m = stage m feed total mass, $m=1, n$
$c_i(x_i)$ = process constraints
C_k = crystal phase impurity weight fraction during sweating
$C_{k,0}$ = initial crystal impurity weight fraction for sweating
C_l = melt phase impurity weight fraction for melt crystallization or sweating
$C_{l,0}$ = initial melt impurity weight fraction for melt crystallization or sweating
C_s = crystal phase impurity weight fraction during melt crystallization
$f(x)$ = objective function
k = melt crystallization or sweating impurity distribution coefficient
k_c, K_c = melt crystallization impurity distribution coefficient, C_s/C_l
k_c^* = bulk melt crystallization impurity distribution coefficient, effective crystallization coefficient
$k_{c,\text{eff}}$ = effective melt crystallization impurity distribution coefficient
k_{eff} = effective or operating impurity distribution coefficient
k_s, K_s = sweating impurity distribution coefficient, C_k/C_l
k_s^* = bulk sweating impurity distribution coefficient, effective sweating coefficient
$k_{s,\text{eff}}$ = effective sweating impurity distribution coefficient
k_c^m = stage m melt crystallization impurity distribution coefficient, $m=1, n$
k_s^m = stage m sweating impurity distribution coefficient, $m=1, n$
M_k = crystal phase total mass during sweating
$M_{k,0}$ = initial crystal total mass for sweating
M_l = melt phase total mass during melt crystallization or sweating
$M_{l,0}$ = initial melt total mass for melt crystallization or sweating
M_s = crystal phase total mass during melt crystallization
q_c = fraction of total mass to crystallizer that is crystallized
q_r = fraction of total residue from crystallizer that is recycled
q_s = fraction of total unsweated crystal mass that is sweated
q_c^m = stage m fraction of total mass to crystallizer that is crystallized, $m=1, n$
q_s^m = stage m fraction of total unsweated crystal that is sweated, $m=1, n$
q_c^* = crystallization fraction maximum
q_s^* = sweating fraction maximum
T = temperature
T_E = eutectic temperature
w = vector of process flowsheet stream impurity weight fractions
w_c = impurity weight fraction of total feed to crystallizer
w^m = stage m vector of process feed impurity weight fractions, $m=0, n$
w_E = system eutectic impurity weight fraction
$w_{E,\text{eff}}$ = system effective eutectic impurity weight fraction
w_f = process feed impurity weight fraction
w_f^m = stage m feed impurity weight fraction, $m=1, n$
w_p = product impurity weight fraction
X = major component weight fraction; also ratio of crystal mass to total mass during sweating, $M_k/M_{k,0}$
x_i = set of independent variables for optimization
X^* = ratio of melt mass to total mass during melt crystallization, $M_l/M_{l,0}$
Y = ratio of mass of impurity in sweated crystal fraction to mass of impurity in initial crystal during sweating, $C_kM_k/(C_{k,0}M_{k,0})$
Y^* = ratio of mass of impurity in melt fraction to mass of impurity in melt feed during melt crystallization, $C_lM_l/(C_{l,0}M_{l,0})$

Greek letters

α = coefficient in objective function
γ = total mass crystallized geometric series variable
ϕ = total impurity crystallized geometric series variable

Literature Cited

Arkenbout, G. J., "Progress in Continuous Fractional Crystallization," *Separation and Purification Methods*, Vol. 7, p. 99, Marcel Dekker, New York (1978).

Atwood, G. R., "Studies in Melt Crystallization," *Separation and Purification Methods*, Vol. 1, p. 297, Marcel Dekker, New York (1972).

Chowdhury, J., "CPI Warm Up to Freeze Concentration," *Chem. Eng.*, 24 (Apr. 25, 1988).

"Countercurrent Cooling Crystallization and Purification Process," Technical Literature, C. W. Nofsinger Co., Kansas City, MO (1991).

Crane, R. L., K. E. Hillstrom, and M. Minkoff, "Solution of the General Nonlinear Programming Problem with Subroutine VMCON," Publication ANL-80-64, Argonne National Laboratory, Argonne, IL (1980).

Fischer, O., S. J. Jancic, and K. Saxer, "Purification of Compounds Forming Eutectics and Solid Solutions by Fractional Crystallization," *Industrial Crystallization*, p. 153, S. J. Jancic and E. J. de Jong, eds., Elsevier Science, New York (1984).

Genck, W. J., "Selection of Crystallizers," *Chem. Process.*, p. 63 (Dec., 1988).

Jancic, S. J., "The Sulzer MWB Fractional Crystallization System," *Sulzer Technical Review*, Sulzer Brothers Limited, Winterthur, Switzerland (1986).

Jancic, S. J., "Fractional Crystallization," *Industrial Crystallization*, p. 57, J. Nyvlt and S. Zacek, eds., Elsevier Science, New York (1989).

Loper, D. E., ed., *Structure and Dynamics of Partially Solidified Systems*, NATO Series E, No. 125, Martinus Nijhoff, Dordrecht, The Netherlands (1987).

Matsuoka, M., "Growth Rates of Organic Binary Crystals from Melts," *Industrial Crystallization*, p. 361, S. J. Jancic and E. J. de Jong, eds., Elsevier Science, New York (1984).

Matz, G., "Fractional Crystallization," *Chem. Ing. Tech.*, **52**, 562 (1980).

Matz, G., "Crystallization from Melts," *Chem. Ing. Tech.*, **52**, 570 (1980).

Matz, G., "Fractional Crystallization," *Ger. Chem. Eng.*, **4**, 63 (1981).

Mayer, M. U., "On the Directed Fractional Crystallization from Falling Films," PhD Thesis, No. 5080, ETH, Zurich (1973).

Mayer, M. U., "Directed Fractional Crystallization from Falling Films," *Verfahrenstechnik*, **8**, 221 (1974).

McCallion, J., "Separation by Freezing," *Chem. Process.*, 33 (Feb., 1989).

Morita, M., and K. Nakamaru, "Industrial Melt Crystallization," *ACHEMA Int. Meeting on Chem. Eng. and Biotechnol. Extracts of the Lecture Groups, Advances and Developments in Mechanical Engineering Packing, Storage and Transport* (1988).

Mutzenberg, A. B., and K. Saxer, "New Process for Material Separation by Crystallization," *DECHEMA Monogr.* (*Dtsch. Ges. Chem. Apparatewes.*), **66**, Nos. 1193-1221, 313 (1970).

Nowicki, B., Z. Wolniewicz, M. Drzazga, and J. Bialek, "Fractional Crystallization in a Vertical Shell-and-Tube Heat Exchanger," *Inz. Apar. Chem.*, **25**, 7 (1986).

Papp, A., and K. Saxer, "MWB Crystallization Process," *Verfahrenstechnik*, **15**, 195 (1981).

"Recent Applications of Freeze Crystallization to Preferential Pollutant Removal and Reuse," Technical Publication, Freeze Technologies Corporation, Raleigh, NC (1988).

Rittner, S., and R. Steiner, "Melt Crystallization of Organic Substances and Its Large Scale Application," *Chem. Ing. Tech.*, **57**, 91 (1985).

Saxer, K., "Fractional Crystallization Process," US Patent 3,621,664 (Nov. 23, 1971).

Saxer, K., "A Large-Scale Industrial Process for Fractional Crystallization," *Chem. Prod.*, p. 28 (Nov., 1980).

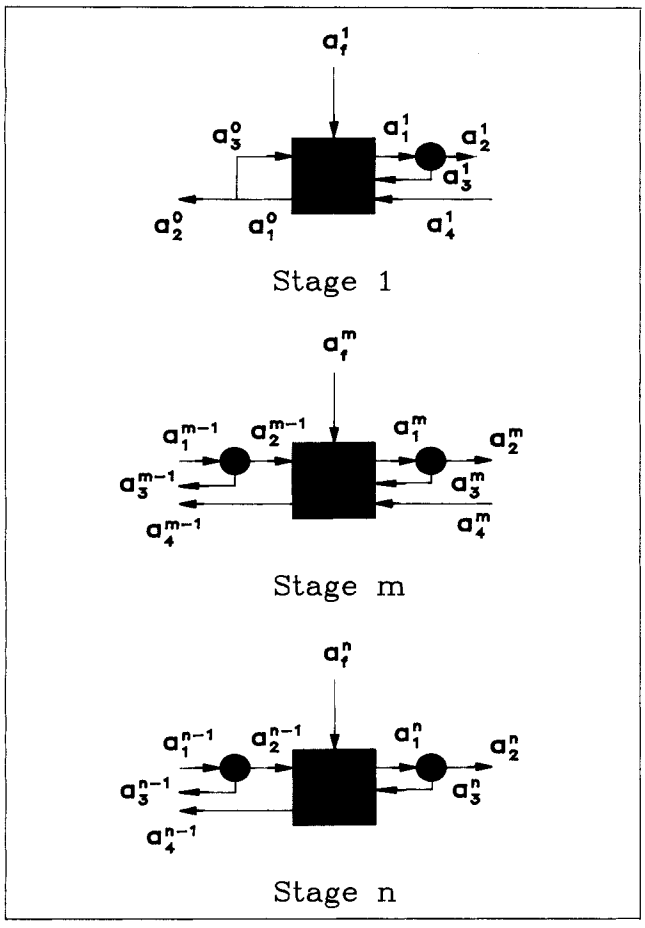

Figure 20. Mass balance diagram for *n*-stage process.

Saxer, K., and A. Papp, "The MWB Crystallization Process," *Chem. Eng. Prog.*, 64 (Apr. 1980).
Shock, R. A. W., "Melt Crystallization, SPS State of the Art Report," SPS SAR 37, Separation Processes Service, Harwell (1981).
Sloan, G. J., and A. R. McGhie, *Techniques of Melt Crystallization, Techniques of Chemistry XIX*, Wiley, New York (1988).
"Sulzer MWB Crystallization Process," Technical Publication, Sulzer Brothers Limited, Buchs, Switzerland (1991).
Ulrich, J., "Purification by Crystallization of Organic Compounds," *Industrial Crystallization*, p. 585, J. Nyvlt and S. Zacek, eds., Elsevier Science, New York (1989).
Wynn, N., "Use Melt Crystallization for Higher Purities," *Chem. Eng.*, 26 (Apr. 28, 1986).
Zief, M., and W. R. Wilcox, eds., *Fractional Solidification 1*, Marcel Dekker, New York (1967).
Zief, M., ed., *Purification of Inorganic and Organic Materials, Techniques of Fractional Solidification*, Marcel Dekker, New York (1969).

Appendix

The reformulation and analyses of the objective function and optima given for the one-stage process can be generalized for the *n*-stage process. Notation refers to Figure 20. Stream total mass balances are:

$$a_1^m - a_2^m - a_3^m = 0, \quad m = 0, \ldots, n \tag{A1}$$

$$a_2^{m-1} - a_4^{m-1} + a_f^m - a_2^m + a_4^m = 0, \quad m = 1, \ldots, n \tag{A2}$$

where $a_4^n = 0$. Since it is unlikely that a multistage separation would require addition of feed to more than one stage,

$$a_f^1 = a_f^2 = , \ldots, = a_f^{t-1} = a_f^{t+1} = , \ldots, = a_f^n = 0 \tag{A3}$$

such that only $a_f^t \neq 0$. Total mass balances in terms of independent variables q_r, q_c^m, and q_s^m are:

$$a_3^0 - (a_2^0 + a_3^0) q_r = 0 \tag{A4}$$

$$a_1^1 - (a_1^0 + a_1^1) q_c^1 = 0 \tag{A5}$$

$$a_1^m - (a_1^m + a_4^{m-1}) q_c^m = 0, \quad m = 2, \ldots, n \tag{A6}$$

$$a_3^m - (a_2^m + a_3^m) q_s^m = 0, \quad m = 1, \ldots, n \tag{A7}$$

Equations A1-A2 and A4-A7 form a system of $4n+2$ equations in $4n+2$ unknowns, and therefore the stream total mass flows can be calculated in terms of independent variables q_r, q_c^m, and q_s^m, $m = 1, n$.

Stream impurity mass balances are:

$$w_1^m a_1^m - w_2^m a_2^m - w_3^m a_3^m = 0, \quad m = 1, \ldots, n \tag{A8}$$

$$w_f^m a_f^m + w_4^m a_4^m + w_2^{m-1} a_2^{m-1} - w_2^m a_2^m - w_4^{m-1} a_4^{m-1} = 0, \quad m = 1, \ldots, n \tag{A9}$$

$$w_1^1 - k_c^1 w_1^0 = 0 \tag{A10}$$

$$w_1^m - k_c^m w_4^{m-1} = 0, \quad m = 2, \ldots, n \tag{A11}$$

$$w_2^m - k_s^m w_3^m = 0, \quad m = 1, \ldots, n \tag{A12}$$

where the stream impurity weight fractions of the residue recycle loop are identical:

$$w_1^0 = w_2^0 = w_3^0 \tag{A13}$$

Equations A8-A13 form a system of $4n+2$ equations in $4n+2$ unknowns, and therefore the stream impurity weight fractions can be calculated in terms of the total mass flows, a_i^m, $i = 1, 4$ and independent variables q_r, q_c^m, and q_s^m, $m = 1, n$.

The objective function to be minimized for the *n*-stage system is:

$$-\alpha a_2^n (1 - w_2^n) + (1 - \alpha) a_1^t \tag{A14}$$

To analyze the objective function and optima, it is convenient to reformulate the mass and impurity balance equations in terms of new independent variables: q_r and impurity weight fractions, w_i^m, $i = 1, 4$, $m = 1, n$. Solving for the stream total mass flows gives:

$$a_2^n = \frac{w_2^0 - w_f^t}{w_2^0 - w_2^n} a_f^t \tag{A15}$$

$$a_2^0 = \frac{w_f^t - w_2^n}{w_2^0 - w_2^n} a_f^t \tag{A16}$$

$$a_2^{m-1} = \frac{(w_f^m - w_4^{m-1}) a_f^m + (w_4^{m-1} - w_2^m) a_2^m + (w_4^m - w_4^{m-1}) a_4^m}{w_4^{m-1} - w_2^{m-1}} \tag{A17}$$

$$a_4^{m-1} = \frac{(w_f^m - w_2^{m-1})a_f^m + (w_2^{m-1} - w_2^m)a_2^m + (w_4^m - w_4^{m-1})a_4^m}{w_4^{m-1} - w_2^{m-1}} \tag{A18}$$

$$a_1^m = \frac{w_3^m - w_2^m}{w_3^m - w_1^m} a_2^m \tag{A19}$$

$$a_3^m = \frac{w_1^m - w_2^m}{w_3^m - w_1^m} a_2^m \tag{A20}$$

$$a_1^0 = \frac{a_2^0}{1 - q_r} \tag{A21}$$

$$a_3^0 = \frac{a_2^0 q_r}{1 - q_r} \tag{A22}$$

for $m = 1, \ldots, n$. It is clear from inspection that the only total mass flows dependent on q_r are a_1^0 and a_3^0. Since the objective function given by expression A14 is independent of a_1^0 and a_3^0, the objective function is independent of q_r. Consequently, there is a one-parameter family of solutions to the optimization problem. Within this family of solutions, only the mass flows in the residue recycle loop are variable.

Manuscript received July 18, 1990, and revision received July 16, 1991.

See NAPS document no. 04885 for 24 pages of supplementary material. Order from NAPS c/o Microfiche Publications, P.O. Box 3513, Grand Central Station, New York, NY 10163. Remit in advance in U.S. funds only $7.75 for photocopies or $4.00 for microfiche. Outside the U.S. and Canada, add postage of $4.50 for the first 20 pages and $1.00 for each of 10 pages of material thereafter, $1.50 for microfiche postage.